PNAS
www.pnas.org

Supplementary Information for

“Contribution of historical precipitation change to United States flood damages”

Frances V. Davenport, Marshall Burke, and Noah S. Diffenbaugh

Corresponding author: Frances Davenport
Email: fvdav@stanford.edu

This PDF file includes:

Supplementary Text

SHELDUS flood damage data

We use flood damage estimates from the Spatial Hazard Events and Losses Database for the United States (SHELDUS) version 17.0 (1), which compiles flood damage estimates from the National Climatic Data Center *Storm Data* publications. We analyze the combined property and crop damage for all events associated with the "Flood" hazard category, which is used to designate non-coastal flooding. We do not include "Coastal Flooding," which is included as a separate category in SHELDUS; a small portion (<1%) of the "Flooding" damages included in the study co-occurred with "Coastal Flooding".

SHELDUS v17.0 includes monthly, county-level flood damage estimates from 1960 through 2017. However, there have been changes in flood damage reporting protocols over this time period, which has resulted in changes in the likelihood of unreported flood damages and the spatial precision of reports over time. For example, the frequency of flood damage reports in SHELDUS increases drastically (and near-linearly) from 1960 to the late 1980s (Fig. S1A). In comparison, the National Flood Insurance Program (NFIP) claims dataset (2), which begins in 1978, shows only a slight increase in the frequency of reports over time. The low frequency of flood damage reports early in the SHELDUS dataset likely indicates that a substantial portion of flood damages were unreported during that period. Beginning in the mid 1980s, changes in the frequency of reports are similar across the two datasets. Based on this comparison, we restrict our analysis of flood damages to the past three decades (1988-2017), when reporting frequency in SHELDUS is most consistent with the NFIP claims dataset.

We also restrict our analysis to state-level damages. Although SHELDUS provides flood damage estimates at the county level, some of the *Storm Data* publications are reported at the state level. SHELDUS splits "statewide" flood damages equally across counties in that state, an arbitrary allocation that does not reflect the true spatial distribution of damage. Inspection of the SHELDUS data suggests that many flood damages that occurred before 1996 were reported at the state level, meaning that county-level estimates before 1996 are less accurate. (This date is also consistent with the transition of the *Storm Data* reports to an electronic database system beginning in 1996.) To avoid potential inaccuracies in county-level estimates, we aggregate all monthly flood damages to the state level.

To evaluate the accuracy of SHELDUS in recording large flood damages, we compare the SHELDUS data with precipitation- and flooding-related events that are part of the NOAA NCEI Billion Dollar Disasters dataset (3). To compare an event between the two datasets, we calculate the total flood damage for all state-months associated with the Billion Dollar Disaster event. On average, the SHELDUS flood damage estimates are ~40% percent of the Billion Dollar Disasters estimates, with a similar bias among the largest and smallest Billion Dollar events (Fig. S1C).

These comparisons suggest that there are uncertainties in the historical record of flood damages in the United States, even after restricting our analysis to the 1988-2017 period and aggregating to the state level. To understand the impacts of errors in the damages data on our analysis, we run two simulations. In the first simulation, we test the impact of missing damages in the data. If there are unreported (i.e. missing) damages, the estimated effect of precipitation on damages is underestimated and has larger uncertainty (Fig. S1B). In this case, both the percent and dollar amount of damages due to precipitation change would be underestimated (see *Impact of historical precipitation trends on flood damages* section). In the second simulation, we test the impact on our results if the dollar value of damages is underestimated (with noise) in the data. If the reported flood damages are underestimated in magnitude, the estimated effect of precipitation on damages remains unbiased but has slightly larger uncertainty (Fig. S1D). In this case, the estimated percent of damages due to precipitation change would be unbiased, but cumulative dollar estimates would be too low. Overall, the presence of reporting errors in the data is unlikely to cause an overestimation of the effect precipitation on flood damage that we report in Figure 3.

Construction of normalized damage variable

To account for increases in exposure specific to each state, we construct a normalized flood damage variable by dividing the flood damages in each month by total state income in that year. The normalized flood damage estimate has units of damage dollars per 100 million dollars of annual state income. Previous studies have used net stock of reproducible fixed assets to normalize natural hazard damages over time (4, 5). Estimates of fixed assets are not available at the annual, state level. However, we find that income is highly correlated with net stock of reproducible assets at the national level, and is highly correlated with estimates of housing values at the state level (Fig. S9).

Around 62% of state-months do not have reported flood damages (Fig. S1E). To account for the possibility that there may have been small, non-zero flood damages during these months, we assign a normalized damage estimate of $1 per $100 million of state income, which is around the 5th percentile of the reported damages in our sample.

Assigning this value also allows for log transformation of the damage variable when fitting the regression model (see below). We test the sensitivity of our results to a number of additional specifications, including (i) using higher or lower assigned values for those months, (ii) excluding months without damages, and (iii) using a value of zero for months without damage and applying an inverse hyperbolic sine transformation, which can be interpreted similarly to a log transformation but allows for zero values. These alternatives lead to slightly higher or lower estimates of the effect of precipitation on damages (Fig. S6); our main specification is in the middle of this distribution, and the interpretation of our results remains unchanged.

Fixed-effects regression models

We use fixed-effects regression models to estimate the causal effect of a change in precipitation on a change in flood damages. As described in the main methods, our initial model is a least-squares log-linear regression model:

$$ln(y_{ilm}) = \delta_{il} + \mu_{im} + \beta P_{ilm} + \varepsilon_{ilm} \quad (1)$$

where y_{ilm} are normalized flood damages in state *i* during month *m* of year *l*, and P_{ilm} is the standardized precipitation anomaly during the same state-month. δ_{il} and μ_{im} are state-year fixed effects and state-calendar month fixed effects, respectively. (Our primary models include state-year and state-month fixed effects, but we also test other combinations of fixed effects, see Fig. S10). The *state-year* fixed effects subtract out year-to-year variations in average damages in each state, allowing us to estimate the effect of monthly precipitation on flood damages after controlling for long-term changes in flood damage in each state. This method requires that a given state has multiple instances of reported flood damage within a year (otherwise, there is no remaining within-year variation to be explained by precipitation). Across all state-years, there is a median of 5 months with reported flood damage, and >87% of state-years have at least two months with reported flood damage. The *state-month* fixed effects subtract out the seasonal cycle in monthly precipitation in each state, as well as the seasonal cycle in flood damages in each state (for example, seasonal differences in crop-related flood damages due to seasonal differences in crop exposure). Due to the plausibly random nature of the remaining variation in monthly precipitation, the estimated value of β in Equation (1) can be interpreted as the causal effect of a change in precipitation on flood damages.

We also test a Poisson regression model using the same set of predictors and fixed effects as Equation 1 (Fig. S10; note that the dependent variable is not log-transformed in the Poisson regression, and months without reported damages are included as zero damages).

We calculate confidence intervals around the estimated coefficients using bootstrap resampling. (The presence of non-Gaussian residuals in the regression model indicates that the coefficient standard errors cannot be used to estimate confidence intervals; Fig. S10.) We use two block bootstrapping methods to account for spatial and temporal dependence. For the “spatial” bootstrap, we resample states (“blocks”) with replacement to generate a new dataset of 48 states. (For the regression models that have a regional interaction term, states are resampled within each region.) We recalculate Equation (1) using the new sample, and repeat this process 1,000 times to generate a set of 1,000 coefficients. The 0.025 and 0.975 quantiles of the calculated coefficients determine the 95% confidence interval around the estimate of β. The temporal bootstrap procedure

is the same, except we resample 3-year blocks with replacement from the original timeseries instead of resampling states. Because the spatial bootstrap yields larger uncertainty ranges than the temporal bootstrap (Fig. S2B), we use the results from the spatial bootstrap as our primary quantification of uncertainty. For models estimating state-specific effects of precipitation (Fig. S2D and Fig. S3), we use the temporal block bootstrap.

We test two non-linear regression models in addition to Equation (1). First, we fit a quadratic model:

$$ln(y_{ilm}) = \delta_{il} + \mu_{im} + \beta_1 P_{ilm} + \beta_2 P_{ilm}^2 + \varepsilon_{ilm} \quad (2)$$

where P_{ilm} is again the standardized precipitation anomaly in state *i* during month *m* of year *l*, and δ_{il} and μ_{im} are state-year fixed effects and state-calendar month fixed effects, respectively. Second, we fit a model with a non-parametric functional form based on precipitation anomaly bins:

$$ln(y_{ilm}) = \delta_{il} + \mu_{im} + \sum \beta_j P_{ilmj} + \varepsilon_{ilm} \quad (3)$$

where P_{ilmj} are dummy variables for *j* precipitation anomaly bins with width of 0.5 standard deviation and ranging from -2.5 to >4 (i.e. [-2.5, -2); [-2, -1.5); …; [3.5, 4); [4, ∞)). In this case, each estimated coefficient, β_j, represents the change in flood damages expected for a month with a precipitation anomaly in bin *j* relative to a month with precipitation in the reference bin (the reference bin represents precipitation anomalies in the [0, 0.5) bin).

We test a number of variations of Equation (1) by including additional interaction terms. We estimate β within different climate regions to see how the effect of precipitation varies spatially, using the equation:

$$ln(y_{ilm}) = \delta_{il} + \mu_{im} + \sum \beta_r P_{ilm} * R_r + \varepsilon_{ilm} \quad (4)$$

where R_r are a set of dummy variables indicating states in each of the nine NCEI climate regions (shown in Fig. 1C) and β_r is the effect of precipitation estimated within each region. Due to the differences in β_r across regions (Fig. 1D), we adopt Equation (4) as our primary regression model for subsequent analyses. We also test Equation (4) using monthly maximum 5-day precipitation instead of total monthly precipitation as the independent variable. Maximum 5-day precipitation also has a positive effect on flood damages; the magnitude of the effect is similar but slightly smaller compared to that of total monthly precipitation.

We quantify seasonal variations in the effect of precipitation on flood damages using the equation:

$$ln(y_{ilm}) = \delta_{il} + \mu_{im} + \sum \beta_{rs} P_{ilm} * R_r * S_s + \varepsilon_{ilm} \quad (5)$$

where S_s are a set of dummy variables that indicate months and β_{rs} is the effect of precipitation on flood damages estimated for each season in each region. December, January, and February are included in winter ("DJF"); March, April and May are included in spring ("MAM"); June, July, and August are included in summer ("JJA"); and September, October, and November are included in autumn ("SON"). For many regions, differences between seasons are small (Fig. 1D), and we continue to use Equation (4) as our primary model. However, we test the sensitivity of the counterfactual damage analysis to using the "seasonal model" (Equation 5) in place of Equation (4), and find that the results are robust to these seasonal differences (Fig. 3B).

There is a possibility that precipitation could have a delayed effect on flood damages. For example, cumulative precipitation over the course of a season could change antecedent soil moisture or streamflow conditions for the current month. We estimate these effects using a distributed lag model:

$$ln(y_{ilm}) = \delta_{il} + \mu_{im} + \beta_1 P_{ilm} + \beta_2 P_{il(m-1)} + \beta_3 P_{il(m-2)} + \varepsilon_{ilm} \quad (6)$$

where $P_{i(m-1)}$ is the precipitation anomaly in state *i* in the previous month, and $P_{i(m-2)}$ is the precipitation anomaly in state *i* two months prior. Precipitation from previous months has a positive but relatively small effect on damages compared to precipitation in the current month (Fig. S2A). We also test the sensitivity to using Equation (6) in place of Equation (4) when calculating the counterfactual damage analysis, and find that the results are robust to these temporal effects (Fig. 3B).

To understand whether the effect of precipitation on damages has changed over time, we estimate β for each decade using the equation:

$$ln(y_{ilm}) = \delta_{il} + \mu_{im} + \sum \beta_d P_{ilm} * D_d + \varepsilon_{ilm} \quad (7)$$

where D_d are a set of dummy variables indicating years in each 10-year period within the analysis (1988-1997, 1998-2007, and 2008-2017). The effect of precipitation on flood damages estimated within each of the three decades (Fig. S2C) is similar to the overall effect estimated using Equation (1), so we do not include separate decadal coefficients in our main regression model.

One caveat is that the equations above estimate only the effect of local (i.e. within-state) precipitation on flood damages, and thus neglect the influence of precipitation from adjacent states that could contribute to fluvial flooding. To estimate the effect of out-of-state precipitation on flood damages, we analyze an example case for Missouri, which contains the outlets of two major river basins: the Missouri River Basin and the Upper Mississippi River Basin (Fig. S3A). We first calculate monthly precipitation in each upstream basin using the 4km gridded PRISM monthly precipitation, and standardize each timeseries based on the mean and standard deviation of monthly precipitation within each basin over the 1986-2005 period. We include precipitation in the upstream basins as additional explanatory variables in the model for Missouri damages, using the equation:

$$ln(y_{lm}^{MO}) = \delta_l + \mu_m + \beta_1 P_{lm}^{MO} + \beta_2 P_{lm}^{MB} + \beta_3 P_{lm}^{UMB} + \varepsilon_{ilm} \quad (8)$$

where y^{MO}_{lm} are flood damages in Missouri during month m of year l, P^{MO}_{lm} is precipitation within the state of Missouri during the same month and year, and P^{MB}_{lm} and P^{UMB}_{lm} are precipitation in the Missouri Basin and Upstream Mississippi Basin, respectively, for the same month and year. In this example case, precipitation outside of the state but within the two upstream basins has a positive – but relatively small and statistically insignificant ($p > 0.1$) – effect on Missouri damages (Fig. S3B). Further, extending this example through the counterfactual damage analysis (see below) shows that accounting for "upstream" precipitation leads to a slightly higher estimate of flood damages due to precipitation change, although the fractional contribution of precipitation change is similar (Fig. S3C). This analysis suggests that our main model may slightly underestimate the effect of precipitation on flood damages by not accounting for the effects of out-of-state precipitation, but that our model using only within-state precipitation captures most of the flood damages associated with precipitation change.

Lastly, we also model the effect of precipitation on the probability that damages occur using the following regression equation:

$$Y_{ilm} = \delta_{il} + \mu_{im} + \beta P_{ilm} + \varepsilon_{ilm} \quad (9)$$

where Y_{ilm} is an indicator variable that takes a value of 1 if damages occurred during a given state-month and a value of 0 otherwise. We fit Equation (9) using least-squares linear regression, but also compare the results to a logistic regression model fit using maximum likelihood estimation (Fig. S11). Equation (9) is informed only by whether or not damages were reported and is insensitive to the magnitude of reported flood damages (including potential biases in the reported magnitude); the fact that this model estimates a relatively large, significant effect of monthly precipitation on the probability of flood damages lends further support to our primary regression results.

Fixed effects regressions are calculated using the "lfe" software package (6) and the "fixest" software package (7), both available in the R computing language. We quantify uncertainty in the estimated response functions for each fixed effects model using the bootstrapping procedures described above.

Observed precipitation trends (Fig. 2 and Fig. S4)

We use quantile regression (8) to calculate historical changes in the 0.50, 0.75, and 0.95 quantiles of the precipitation distribution. We use this approach to identify trends in different portions of the precipitation distribution that contribute to flood damages (Fig. 1B), as these may differ in sign or magnitude from trends in mean precipitation (9, 10). We calculate trends for each state over the 90-year period from 1928-2017 (Fig. S4). Fig. S5A shows the range of trends calculated using earlier or later starting years; we find that the distribution of trends is quite stable for starting years before the mid-20th century, and that the range of trends increases for trends beginning between the mid-20th century and late-20th century. Quantile regressions are calculated using the "quantreg" software package (11) available in the R computing language.

We calculate statistical significance of the observed precipitation trends using a moving block bootstrap (12), following the approach of Singh et al. (13). We use a block size of 12 months

so that each year in the resampled time series contains each calendar month. For each bootstrap replicate, we randomly sample 12-month blocks from the original time series, placing them in the order they are sampled to create a new time series with the same length as the original. We recalculate trends at the 0.50, 0.75, and 0.95 quantile for the new time series, repeating the bootstrapping 1,000 times to produce a distribution of trends. We use the empirical quantiles of this distribution to determine the probability of the observed trend under random variability. We assign statistical significance at the $p < 0.10$ level if the empirical quantile of the observed trend is less than 0.05 or greater than 0.95, and statistical significance at the $p < 0.05$ if the empirical quantile of the observed trend is less than 0.025 or greater than 0.975.

To enable direct comparison with climate model simulations, we also calculate historical trends in monthly precipitation on the 2.5x2.5 degree geographical grid used in the IPCC AR5 (Fig. 2). We regrid the 4km PRISM monthly precipitation to the 2.5x2.5 degree grid, and then calculate the standardized monthly precipitation time series for each grid cell. We also calculate trends in monthly maximum 5-day precipitation using the CLIMDEX HadEX3 monthly "Rx5day" data (14). (The PRISM daily precipitation data, which we use to test sensitivity of the regression model, begins in 1981, so we use the CLIMDEX Rx5day data to calculate long-term trends). We regrid the 1.875 degree x 1.25 degree CLIMDEX HadEX3 data to the 2.5x2.5 degree grid, and then calculate the standardized monthly maximum 5-day precipitation time series for each grid cell using the procedures described above.

Calculating "counterfactual" precipitation

We create a counterfactual precipitation time series by removing the observed precipitation trends. To account for non-uniform trends in the distribution of precipitation, we calculate trends for each decile of the distribution. For each state, we first calculate the threshold values for each decile (i.e. 10^{th} percentile value, 20^{th} percentile value, etc.) as a function of time. Each month of the historical time series is then assigned to a decile based on these threshold values. For example, a monthly precipitation anomaly between the 10^{th} and 20^{th} percentile threshold values for that year falls in the second decile bin. From each monthly precipitation anomaly, we subtract the trend calculated for the percentile in the middle of the decile. For example, in the case of the second decile bin, we calculate the trend in the 15^{th} percentile of the distribution and subtract that trend from all monthly precipitation anomalies that fall in that decile bin. The distributions of observed and counterfactual monthly precipitation anomalies (pooled across states) are shown in Fig. S8. Quantile regressions for each decile are calculated using the "quantreg" software package (11) available in the R computing language.

Estimating uncertainty in the counterfactual scenario

We calculate a 95% confidence range for our estimate of cumulative counterfactual damages based on (i) uncertainty in the regional regression coefficients and (ii) uncertainty in the observed precipitation trends. We calculate uncertainty in the precipitation trends by randomly removing 20% of the years from our dataset and recalculating the observed trends in each state (Fig. S5B). By removing the same years across all states, we preserve the observed spatial dependence between states. We repeat this process 10,000 times. For each of the 10,000 iterations, we re-calculate the counterfactual damages using the 1,000 bootstrapped estimates of the regional regression coefficients, creating a distribution of 10 million counterfactual damage estimates. We calculate the 0.025 and 0.975 empirical quantiles of this distribution to estimate the 95% confidence range for cumulative damages contributed by precipitation changes.

We evaluate the sensitivity of the counterfactual damage analysis to a number of methodological choices by repeating the steps above using other regression models, and using precipitation trends over different time periods. To test the sensitivity to the regression model specification, we replace the regional regression model with (i) the regional model with lagged precipitation effects (Eq. 6), (ii) the regional-seasonal interaction model (Eq. 5), (iii) a linear model for all regions (Eq. 1), and (iv) a quadratic model for all regions (Eq. 2). As described above, we also test the sensitivity to using the regional regression model (Eq. 4) with various dependent variable transformations (Fig. S6). Further, we estimate the sensitivity to the precipitation trends by

repeating the analysis using precipitation trends starting in 1898, 1908, 1918, 1938, 1948, and 1958. The various alternatives lead to slightly higher or lower estimates of counterfactual damage, with our main result falling in the middle of the distribution (Fig. 3B-C; Fig. S6).

Comparison of observations with climate model experiments

We compare the observed precipitation trends with climate model simulations from the Coupled Model Intercomparison Project (CMIP5) (15). We analyze monthly precipitation from the CMIP5 archive, as well as monthly maximum 5-day precipitation ("Rx5day") from the CLIMDEX CMIP5 archive (16, 17). We analyze the 24 simulations included in the IPCC Fifth Assessment Report (IPCC AR5) (18) that also have monthly maximum 5-day precipitation available through the CLIMDEX CMIP5 archive (see list of models and simulations in Table S1). In using an ensemble of global climate model simulations, we can evaluate how the observed trends compare to the mean response to increased climate forcing. In order to evaluate changes in precipitation over the historical period used for the flood damage analysis (1988-2017), we combine the Historical simulations, which end in 2005, with the 2006-2017 period of the corresponding Representative Concentration Pathway 8.5 (RCP8.5) forcing simulations. In the period since 2005, the RCP8.5 "high emission" forcing scenario closely resembles the observed greenhouse gas emissions (19). Combing these simulations yields a 30-year "recent historical" timeseries for each realization. We use the 1860-1920 period of each Historical simulation to calculate the baseline 50^{th}, 75^{th}, 95^{th}, and 99^{th} percentiles of monthly precipitation. While the Natural simulations (which do not include anthropogenic climate forcing) could provide an alternative baseline, the Natural simulations end in 2005 (and hence only cover 60% of the recent historical period). Further, not all of the Historical simulations have a corresponding Natural simulation.

We analyze all climate model output on the 2.5x2.5 degree geographical grid used in the IPCC AR5. We standardize the monthly precipitation and monthly maximum 5-day precipitation time series in each grid cell in each simulation using the mean and standard deviation of the Historical simulation over the 1986-2005 period.

To quantify how precipitation has changed under historical anthropogenic climate forcing, we calculate probability ratios between the recent historical and baseline periods, which is a common approach in the attribution literature to assess how the frequency of extreme events has changed (20–22). To do this, we calculate the number of times the baseline 50^{th}, 75^{th}, 95^{th}, and 99^{th} percentile monthly precipitation and monthly maximum 5-day precipitation thresholds were exceeded in each grid cell during the recent historical period of each simulation. (The threshold values are calculated separately for each grid cell in each simulation). We then count the number of exceedances across all simulations (separately for each threshold and grid cell). We determine the change in probability of occurrence (Fig. 4) by calculating the ratio of actual exceedances in 1988-2017 to the number of exceedances that would be expected based on the 1860-1920 percentile threshold. For example, exceeding the 95^{th} percentile in 36 months over 30 years (10% of the time) is twice the number of expected exceedances (18 months, or 5% of the time), which corresponds to a probability ratio of 2 compared to the baseline.

Projections of future precipitation change

In order to quantify the response to higher levels of anthropogenic climate forcing (23–25), we calculate the change in the 50^{th}, 95^{th}, and 99^{th} percentiles of monthly total and maximum 5-day precipitation for two future periods (2046-2065 and 2081-2100) and for two future scenarios (RCP8.5 and RCP2.6). For this analysis, we use the 17 climate models that have both RCP8.5 and RCP2.6 simulations (see Table S1). RCP8.5 and RCP2.6 are the two scenarios featured in the assessment of impacts, adaptation and vulnerability in the IPCC AR5 (18). The RCP8.5 "high emission" scenario tracks the trajectory of global carbon dioxide emissions in the first decade following the end of the CMIP5 Historical simulations, and is the highest forcing scenario in CMIP5. In comparison, the RCP2.6 "low emissions" scenario is consistent with the UN Paris Agreement 1.5-2°C global warming targets (15).

We calculate future changes relative to the recent historical period. To do this, we calculate the quantile thresholds in each simulation over each time period (1988-2017, 2046-2065, and 2081-2100). We then calculate the difference between the 50^{th}, 95^{th}, and 99^{th} percentile thresholds in each future period and the recent historical period (separately for each simulation pair). We calculate the mean difference across all simulations to represent the ensemble mean change in each future period. We present the projected changes in standardized precipitation units for each percentile threshold. Using standardized precipitation units to quantify future change enables direct comparison with our regression model results and allows the impact of future precipitation change on the cost of flood damages to be interpreted more easily.

A

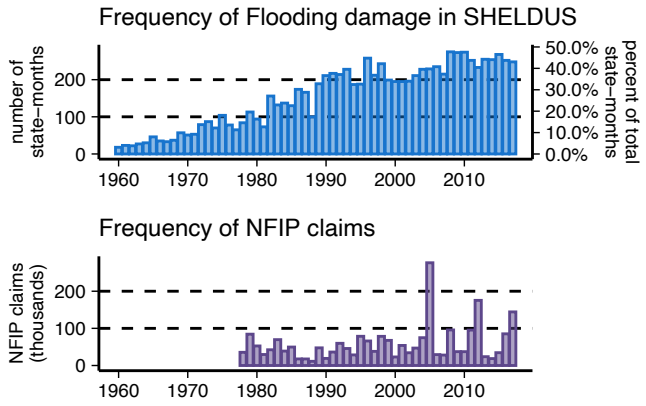

B

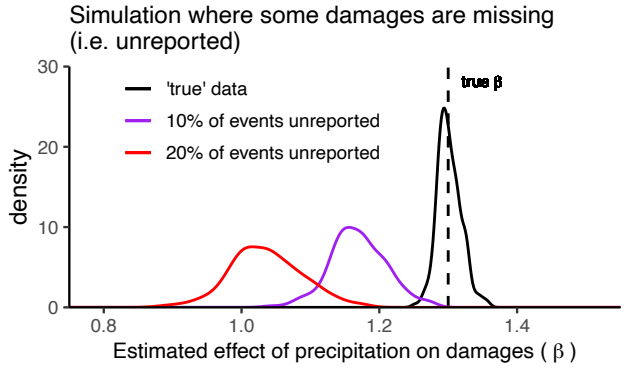

C

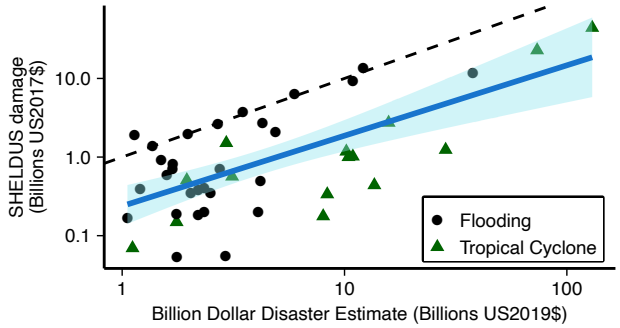

D

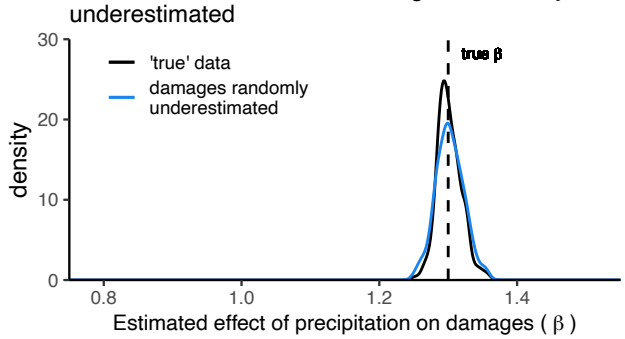

E

region	events	damage (billions)	percent of damage
Northwest	268	$2.31	1.16%
West	266	$8.05	4.05%
Southwest	454	$2.66	1.34%
Northern Rockies Plains	447	$7.47	3.76%
South	1152	$66.83	33.6%
Upper Midwest	534	$30.58	15.4%
Central	1372	$31.41	15.8%
Southeast	988	$11.74	5.91%
Northeast	1147	$37.77	19.0%

F

season	events	damage (billions)	percent of damage
DJF	995	$12.30	6.19%
MAM	1747	$30.31	15.2%
JJA	2670	$116.37	58.5%
SON	1216	$39.84	20.0%

G

Proportion of months with flood damage (1988-2017):

All	**0.38**	Idaho	0.27	Michigan	0.34	New York	0.64	Tennessee	0.58
Alabama	0.43	Illinois	0.47	Minnesota	0.31	North Carolina	0.47	Texas	0.76
Arizona	0.31	Indiana	0.53	Mississippi	0.61	North Dakota	0.21	Utah	0.31
Arkansas	0.52	Iowa	0.52	Missouri	0.49	Ohio	0.63	Vermont	0.33
California	0.48	Kansas	0.41	Montana	0.21	Oklahoma	0.38	Virginia	0.51
Colorado	0.3	Kentucky	0.59	Nebraska	0.39	Oregon	0.18	Washington	0.3
Connecticut	0.16	Louisiana	0.53	Nevada	0.26	Pennsylvania	0.59	West Virginia	0.52
Delaware	0.09	Maine	0.23	New Hampshire	0.22	Rhode Island	0.11	Wisconsin	0.32
Florida	0.48	Maryland	0.29	New Jersey	0.2	South Carolina	0.36	Wyoming	0.18
Georgia	0.49	Massachusetts	0.32	New Mexico	0.34	South Dakota	0.26		

Figure S1. Overview of flood damage data. **A,** Number of state-months with reported damage in SHELDUS (top, blue) and number of NFIP flood insurance claims (bottom, purple) each year. Note that NFIP claims include both inland and coastal flooding. **B,** Effect of missing damages on estimated regression coefficient. **C,** Comparison of flood damage estimates from SHELDUS with the NCEI Billion Dollar Disasters data. The Billion Dollar Disasters data begins in 1980, and only events described as resulting from rainfall and non-coastal flooding are shown. SHELDUS damages are aggregated for the states and months listed for each Billion Dollar Disaster event. Dashed black line shows the 1:1 line, and the blue line shows a linear regression model fit between damages from the two datasets. **D,** Effect of underestimated damages on estimated regression coefficient. **E,** Distribution of SHELDUS flood damages by region. **F,** Distribution of SHELDUS flood damages by season. **G,** proportion of months with reported flood damages overall and within each state.

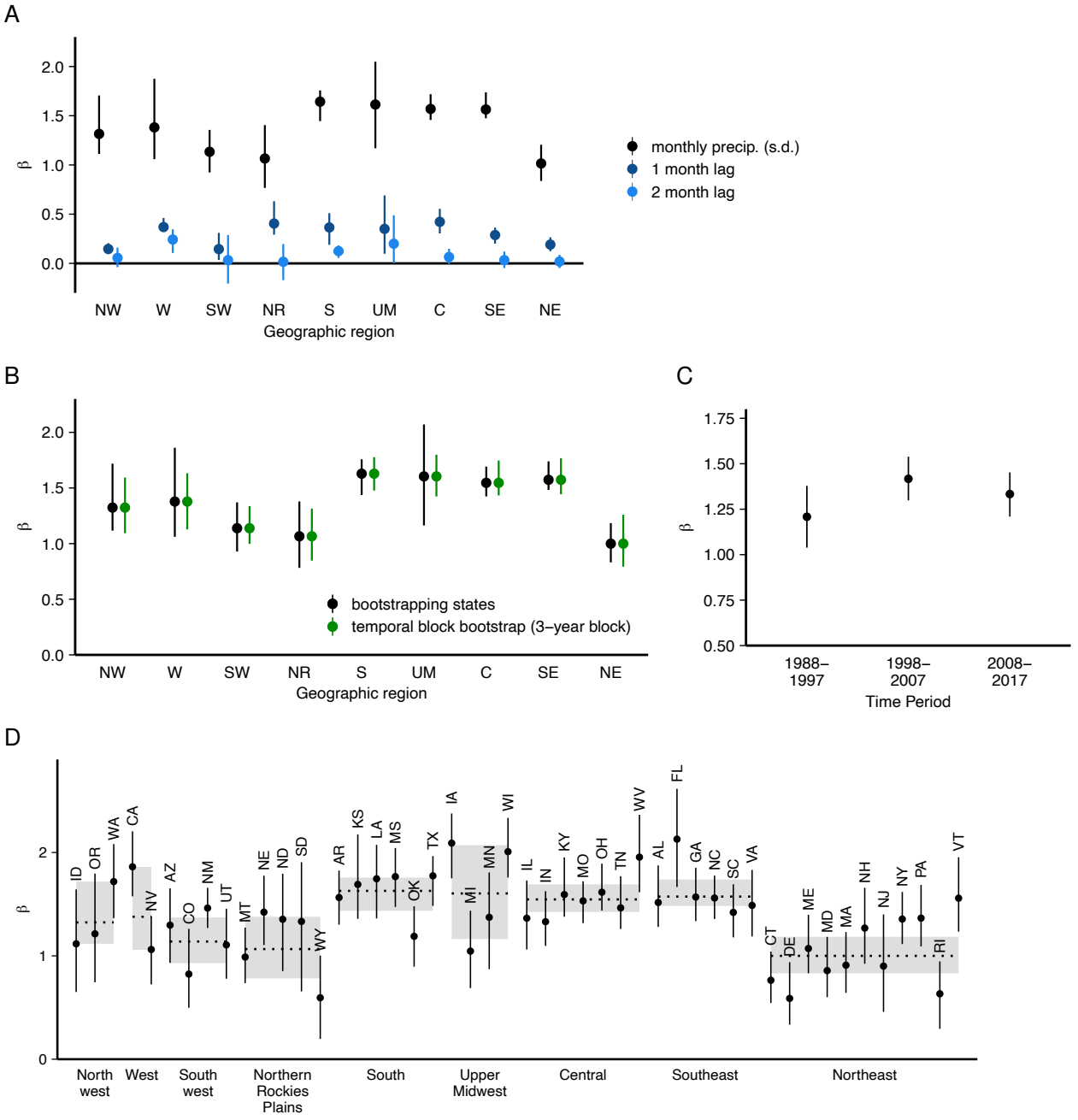

Figure S2. Alternative regression model specifications. **A,** Effect of precipitation on flood damages for precipitation from the present month (black), precipitation from the prior month (dark blue), and precipitation from two months prior (lighter blue), measured as the change in ln(normalized damages) per standard deviation change in monthly precipitation anomaly. Points show the median coefficient estimates, and vertical lines indicate the 95% CI around each point, estimated by bootstrapping states within each region. **B,** Uncertainty around the effect of precipitation on monthly flood damages using a spatial bootstrap (black) and a temporal block bootstrap with 3-year blocks (green). Vertical lines indicate the 95% CI around the point estimates using each bootstrapping method. **C,** Effect of precipitation on monthly flood damages for three 10-year time periods: 1988-1997, 1998-2007, and 2008-2017. **D,** Effect of precipitation on monthly flood damages within each state. Points show the median coefficient estimate for each state, and vertical lines indicate the 95% CI around each point. Black dotted lines indicate the median coefficient estimate for each region, and gray shading shows the 95% CI around the regional coefficients (same as Fig. 1d). For the individual state models, uncertainty is calculated using a temporal block bootstrap with 3-year blocks.

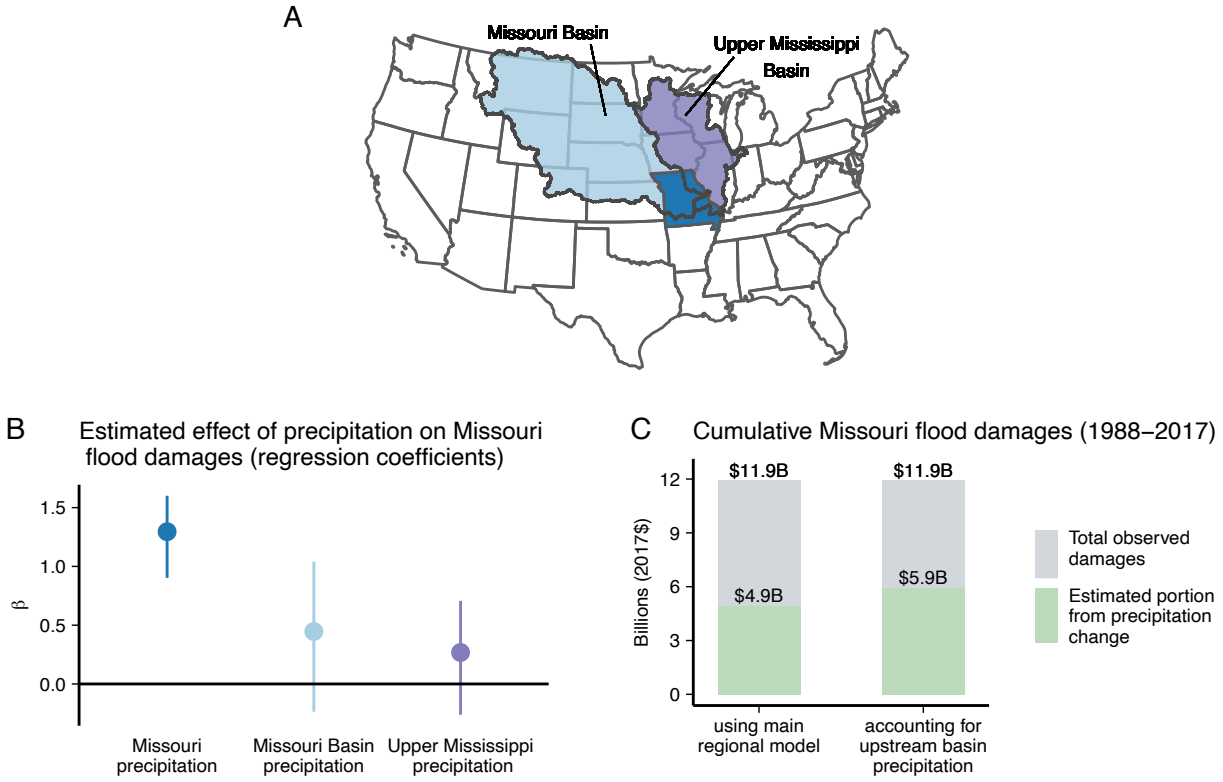

Figure S3. Effect of basin-scale precipitation on flood damages. **A,** Map showing the state of Missouri (dark blue) and two HUC-02 level watersheds that drain into Missouri: the Missouri River Basin (light blue) and the Upper Mississippi Basin (purple). **B,** Estimated effect of precipitation on Missouri flood damages, modeled with the equation $ln(y_{l,m}^{MO}) = \delta_l + \mu_m + \beta_1 P_{l,m}^{MO} + \beta_2 P_{l,m}^{MB} + \beta_3 P_{l,m}^{UMB}$, where $y_{l,m}^{MO}$ are flood damages in Missouri during year l and month m, $P_{l,m}^{MO}$ is the precipitation within the state of Missouri during the same year and month, $P_{l,m}^{MB}$ is precipitation in the Missouri Basin (excluding the state of Missouri) during the same year and month, and $P_{l,m}^{UMB}$ is precipitation within the Upper Mississippi Basin (excluding the state of Missouri) during the same year and month, and δ_l and μ_m are sets of year and month fixed effects, respectively. Points indicate the median estimate, and lines indicate the 95% confidence interval, calculated using a temporal block bootstrap with 3-year block size (see Methods). **C,** Estimated impact of precipitation change on the cumulative flood damages in Missouri from 1988 through 2017 using the main regional model and in the model accounting for upstream basin precipitation (as described in B).

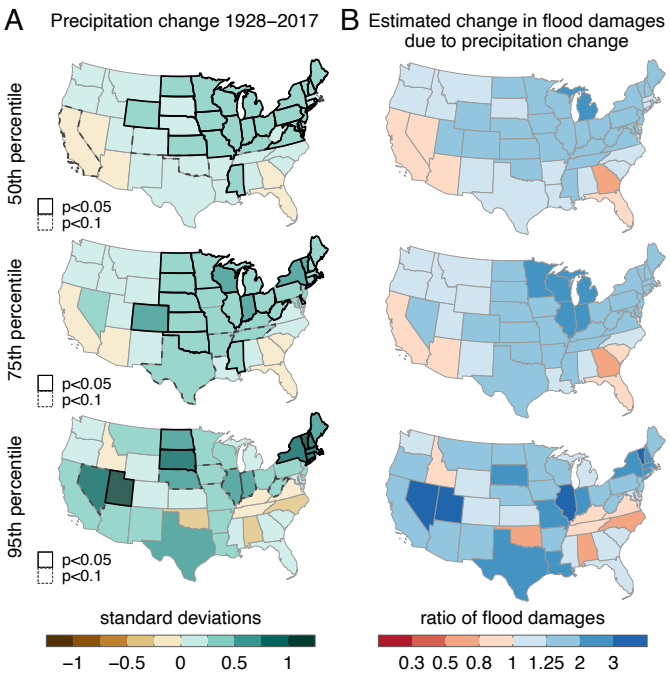

Figure S4. Historical precipitation change and estimated effect on monthly flood damages. **A,** change in the 50th, 75th, and 95th percentile of state-level monthly precipitation due to historical precipitation trends from 1928-2017, measured in standard deviations. Trends are calculated using quantile regression. The border around each state indicates the probability of the observed trend under random chance (see *Supplementary Text*): light gray ($p > 0.1$), dashed gray ($0.05 < p < 0.1$), dark gray ($p < .05$). **B,** Estimated change in monthly flood damages due to the precipitation changes shown in A and the effect of precipitation on damages estimated with our main regression model (equation 4; Fig. 1C). Estimated change in damages is expressed as the ratio of expected damages with precipitation change to those without precipitation change. At the 0.50, 0.75, and 0.95 quantiles shown, this can be thought of as the change in expected damages from monthly precipitation that has 50%, 25%, and 5% probability of occurrence, respectively.

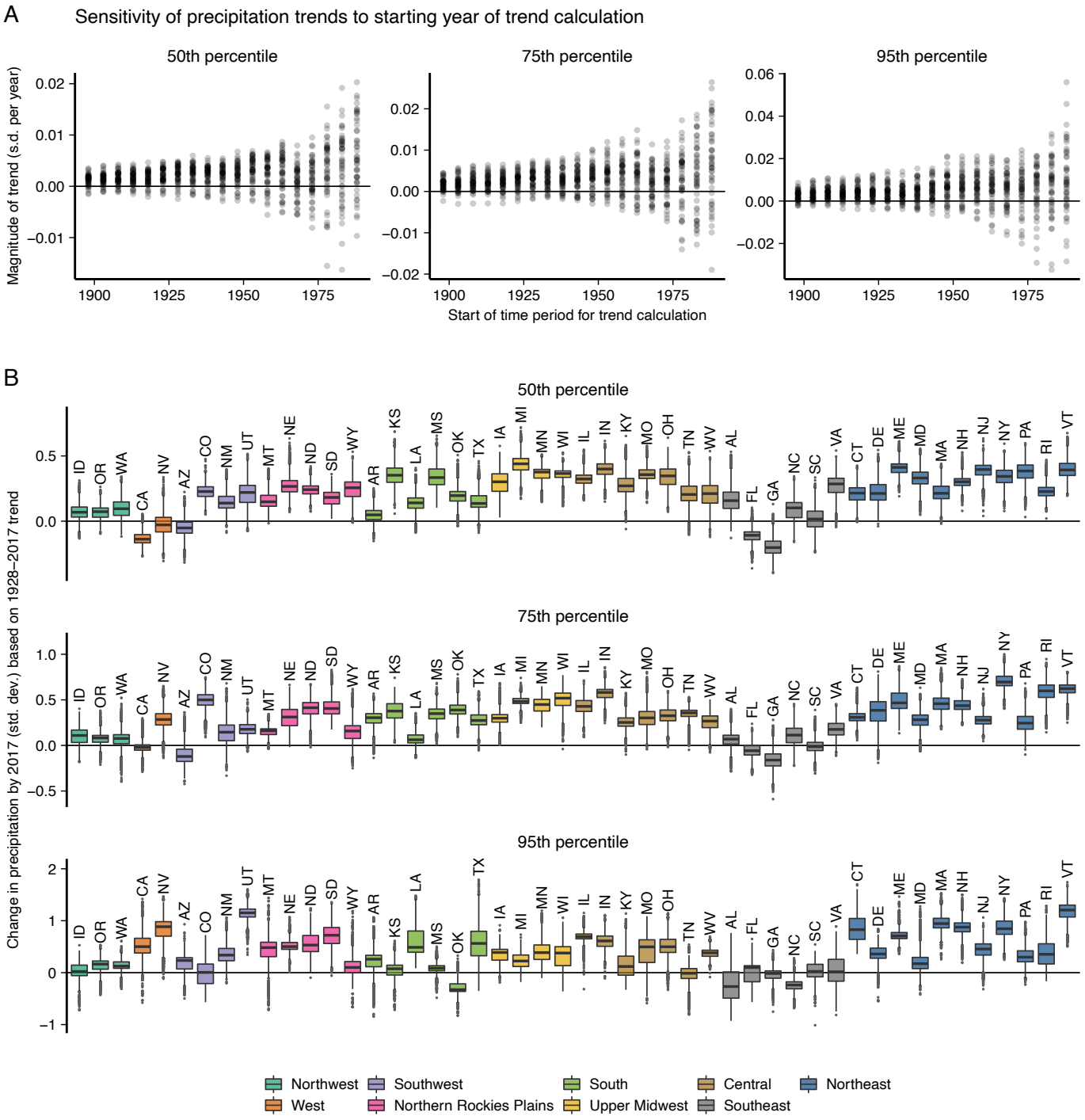

Figure S5. Uncertainty in state-level precipitation trends. **A,** distribution of the 48 state-level precipitation trends at three precipitation percentiles (50th percentile, 75th percentile, and 95th percentile) depending on the length of the trend time period. The length of the time periods for the trends shown range from 120 years (1898-2017) to 30 years (1988-2017), at increments of 5 years. **B,** distribution of 1928-2017 precipitation trends for each state, determined by randomly resampling 80% of years and recalculating trends for each resampled set. Resampling is repeated 10,000 times. The vertical axis shows the change in precipitation in 2017 as a result of the trend, calculated by multiplying the trend magnitude (in s.d. per year) by the trend length (90 years). The middle line of each boxplot shows the change associated with the median trend for each state, the top and bottom of the boxplots show the 25th percentile and 75th percentile of the distribution, and the whiskers extend to 1.5 times the interquartile range (defined as the distance between the 25th and 75th percentiles). Points show trends that lie above or below the whiskers.

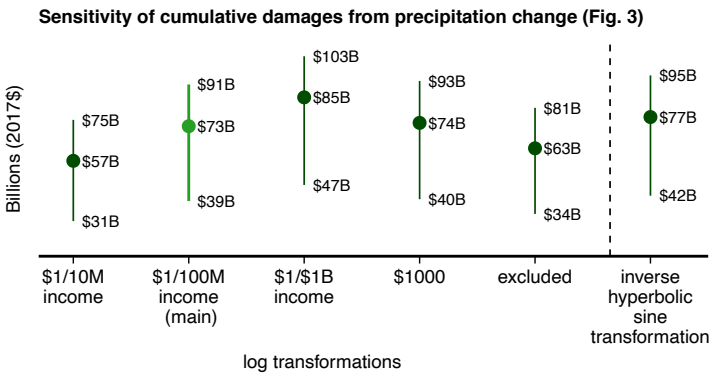

Figure S6. Alternative treatment of months without damage. Same as Figure 3B-C, but showing the sensitivity to treatment of months without reported damage. From left to right: assigning $1/$10 million in state income for months without damage ("$1/$10M income"); assigning $1/$100 million in state income for months without damage ("$1/$100M income"; this is the main value used in the paper and in Figure 3A); assigning $1/$1 billion in state income for months without damage ("$1/$1B income"); assigning $1000 for months without damage and normalizing by state income for all months ("$1000"); excluding months without damage ("excluded"); and using a value of $0 for months without damage, but using an inverse hyperbolic sine transformation instead of a log transformation for the normalized damage variable ("inverse hyperbolic sine transformation").

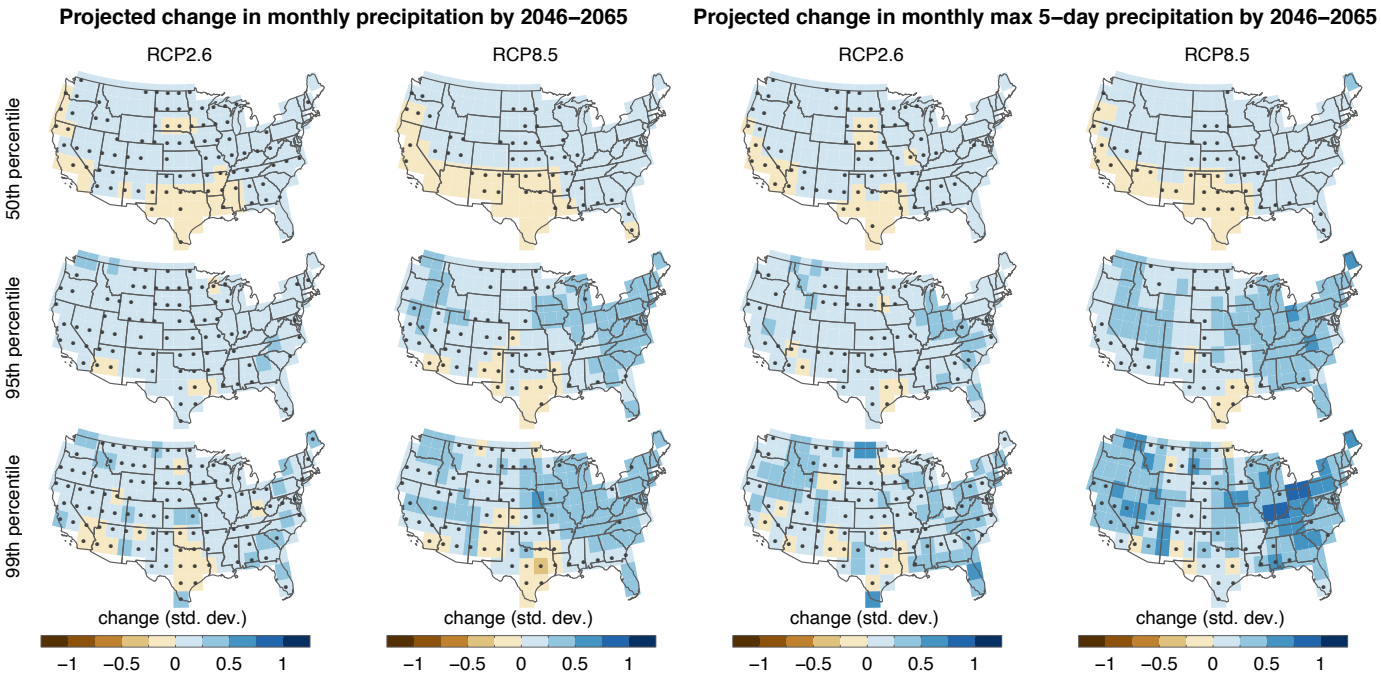

Figure S7. Same as Fig. 5A-D, but for projected change by 2046-2065.

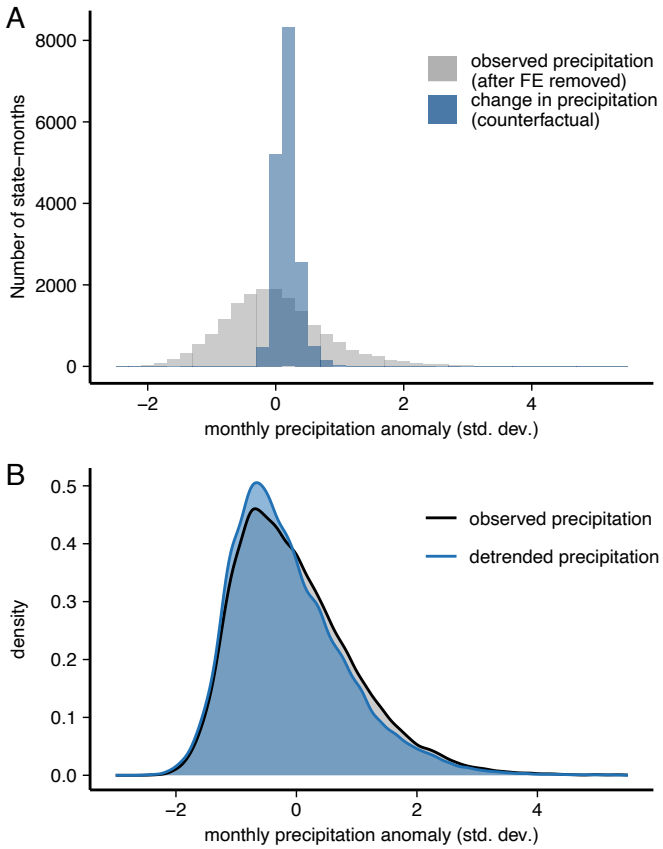

Figure S8. Observed and counterfactual precipitation distributions. **A,** Distribution of 1988-2017 monthly precipitation anomalies after accounting for state-year and state-month fixed effects (gray bars), and the distribution of monthly precipitation shifts calculated under the counterfactual scenario (blue bars). Observations are pooled across all 48 states. The gray distribution represents the range of "within-state" precipitation variability after accounting for fixed effects, and the blue distribution represents the magnitude of the counterfactual "treatment". **B,** Probability density functions of the original distribution of 1988-2017 observed monthly precipitation anomalies (black line) and the calculated distribution of 1988-2017 counterfactual monthly precipitation anomalies (blue line). Observations are pooled across all 48 states.

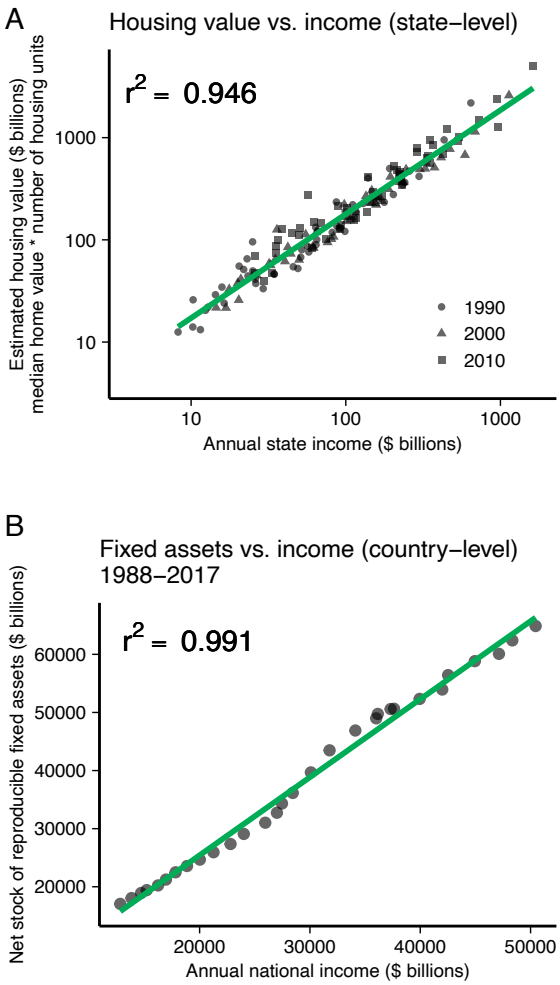

Figure S9. Correlation between income and housing values. **A,** Estimated state housing values vs. state-level annual income. Points show data for each of the 48 states in 1990, 2000, and 2010, and the green line shows the linear relationship. Estimated housing values are calculated by multiplying the median home value in each state by the number housing units in the same state. State income values are provided by the U.S. Bureau of Economic Analysis and housing data comes from the U.S. Census and American Community Survey. **B,** National estimate of net-stock of reproducible fixed assets vs. national income for each year from 1988-2017 (points indicate individual years, and the green line shows the linear relationship between the two). Income and fixed assets come from the U.S. Bureau of Economic Analysis.

A Sensitivity of monthly precipitation coefficient to fixed effect combinations

	state-year FE, state-month FE (eq. 1)	none	state-year FE	state FE, year FE	state FE, year FE, state-month FE
	(1)	(2)	(3)	(4)	(5)
monthly precip (s.d.)	1.323***	1.457***	1.428***	1.444***	1.354***
	(0.021)	(0.019)	(0.019)	(0.018)	(0.020)
State-year FE	Yes	No	Yes	No	No
State FE	No	No	No	Yes	Yes
Year FE	No	No	No	Yes	Yes
State-month FE	Yes	No	No	No	Yes
R^2 (projected model)	0.213	0.254	0.267	0.263	0.214
Degrees of freedom	15311	17278	15839	17202	16627
Observations	17,280	17,280	17,280	17,280	17,280

Notes: standard errors are shown in parentheses; *p<0.1; **p<0.05; ***p<0.01

B Comparison of log-linear (OLS) and Poisson models

	OLS	Poisson
monthly precip (s.d.) coefficient	1.323	1.758
(95% CI)	(1.21, 1.43)	(1.30, 2.24)
State-year FE	Yes	Yes
State-month FE	Yes	Yes
Observations	17,280	15,633

C Regional monthly precipitation coefficients

	main regional model (eq. 4)
monthly precip (Northwest)	1.324 (0.105)***
monthly precip (West)	1.378 (0.110)***
monthly precip (Southwest)	1.139 (0.072)***
monthly precip (Northern Rockies Plains)	1.066 (0.076)***
monthly precip (South)	1.629 (0.055)***
monthly precip (Upper Midwest)	1.604 (0.086)***
monthly precip (Central)	1.546 (0.051)***
monthly precip (Southeast)	1.574 (0.058)***
monthly precip (Northeast)	1.000 (0.038)***
State-year FE	Yes
State-month FE	Yes
R^2 (projected model)	0.222
Degrees of Freedom	15303
Observations	17,280

Notes: standard errors are shown in parentheses; *p<0.1; **p<0.05; ***p<0.01

D

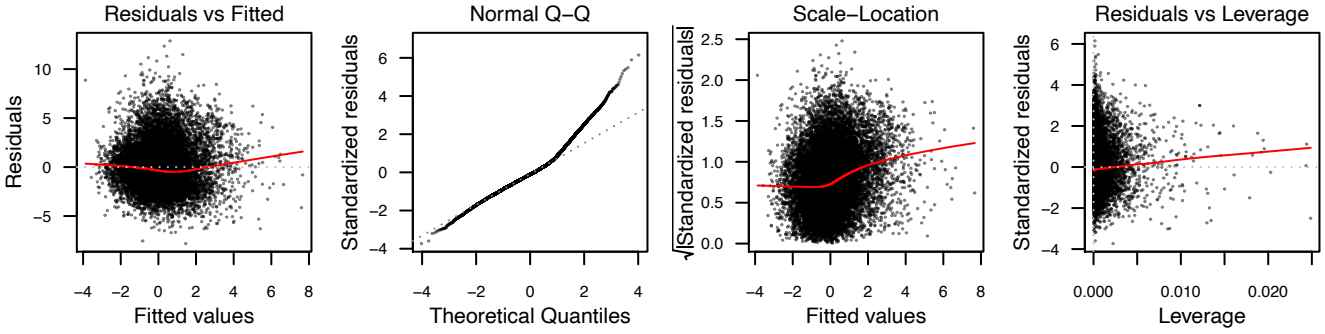

Figure S10. Details of regression model fits. **A,** sensitivity of model coefficients and model fit to different fixed effect combinations. Standard errors shown are calculated by the lfe statistical software package, but uncertainty estimates in the paper are calculated by bootstrapping (see Methods). **B,** comparison of monthly precipitation coefficients using a log-linear model and a Poisson regression model. The Poisson model is fit using maximum likelihood estimation. For both models, 95% confidence intervals shown in parentheses are calculated by bootstrapping states. **C,** monthly precipitation coefficients estimated using the main regional regression model. Standard errors shown are calculated by the lfe statistical software package, but uncertainty estimates in the paper are calculated by bootstrapping (see Methods). **D,** diagnostic plots for the main regional regression model shown in C and Figure 1A.

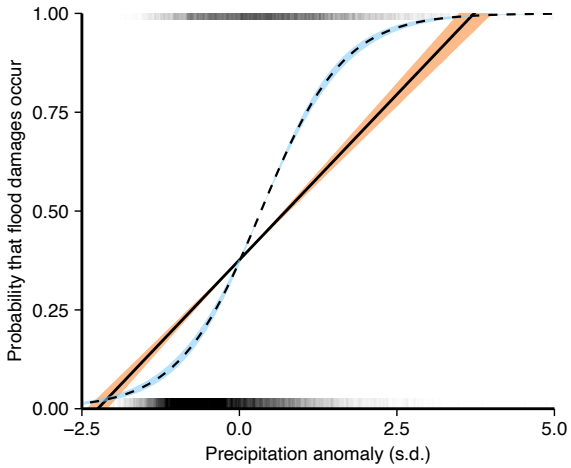

Figure S11. Effect of state-level precipitation on the probability of damages. Estimated relationship between the probability of flood damages and monthly precipitation anomalies at the state-level using a linear (OLS) model (solid line, orange shading) and a logit model (dashed line, blue shading). Shading shows the 95% confidence intervals estimated by bootstrapping states. Response functions are centered at the mean monthly precipitation anomaly (0.0425) and the mean probability of damages (0.384). Vertical bars at y = 1 and y = 0 show the density of months with and without damages across monthly precipitation anomalies.

Table S1. CMIP5 models and simulations

	Fig. 4 historical and RCP8.5	Fig. 5 and Fig. S7 RCP2.6 and RCP8.5
ACCESS1-0	r1i1p1	–
bcc-csm1-1	r1i1p1	r1i1p1
CanESM2	r1i1p1	r1i1p1
CCSM4	r1i1p1	–
CMCC-CM	r1i1p1	–
CMCC-CMS	r1i1p1	–
CNRM-CM5	r1i1p1	r1i1p1
CSIRO-Mk3-6-0	r1i1p1	r1i1p1
GFDL-CM3	r1i1p1	r1i1p1
GFDL-ESM2G	r1i1p1	r1i1p1
GFDL-ESM2M	r1i1p1	r1i1p1
HadGEM2-CC	r1i1p1	–
HadGEM2-ES	r2i1p1	r2i1p1
inmcm4	r1i1p1	–
IPSL-CM5A-LR	r1i1p1	r1i1p1
IPSL-CM5A-MR	r1i1p1	r1i1p1
IPSL-CM5B-LR	r1i1p1	–
MIROC-ESM	r1i1p1	r1i1p1
MIROC-ESM-CHEM	r1i1p1	r1i1p1
MIROC5	r1i1p1	r1i1p1
MPI-ESM-LR	r1i1p1	r1i1p1
MPI-ESM-MR	r1i1p1	r1i1p1
MRI-CGCM3	r1i1p1	r1i1p1
NorESM1-M	r1i1p1	r1i1p1
Total	24	17

Supplementary References

1. Center for Emergency Management and Homeland Security, “The Spatial Hazard Events and Losses Database for the United States, Version 17.0 [Online Database].” (2018).
2. F. E. M. Agency, FIMA NFIP Redacted Claims Data Set (2019).
3. NCEI, Billion-Dollar Weather/Climate Events. (2019).
4. M. W. Downton, J. Z. B. Miller, R. A. Pielke, Reanalysis of U.S. National Weather Service Flood Loss Database. *Nat. Hazards Rev.* **6**, 13–22 (2005).
5. J. Pielke, Roger A., *et al.*, Normalized Hurricane Damage in the United States : 1900 – 2005. *Nat. Hazards Rev.* **9**, 29–42 (2008).
6. S. Gaure, lfe: Linear group fixed effects. *R J.* **5**, 104–117 (2013).
7. L. Bergé, Efficient estimation of maximum likelihood models with multiple fixed-effects: the R package FENmlm. *CREA Discuss. Pap.* (2018).
8. R. Koenker, G. Bassett, Regression Quantiles. *Econometrica* **46**, 33 (1978).
9. S. K. Min, X. Zhang, F. W. Zwiers, G. C. Hegerl, Human contribution to more-intense precipitation extremes. *Nature* **470**, 378–381 (2011).
10. R. P. Allan, B. J. Soden, Atmospheric Warming and the Amplification of Precipitation Extremes. *Science (80-.).* **321**, 1481–1485 (2008).
11. R. Koenker, Quantreg: Quantile regression. R package version 5.42.1 (2019).
12. H. R. Kunsch, The jacknife and the bootstrap for general stationary observations. *Ann. Stat.* **17**, 1217–1241 (1989).
13. D. Singh, M. Tsiang, B. Rajaratnam, N. S. Diffenbaugh, Observed changes in extreme wet and dry spells during the south Asian summer monsoon season. *Nat. Clim. Chang.* **4**, 456–461 (2014).
14. R. J. H. Dunn, *et al.*, Development of an Updated Global Land In Situ - Based Data Set of Temperature and Precipitation Extremes : HadEX3 Journal of Geophysical Research : Atmospheres. 1–28 (2018).
15. K. E. Taylor, R. J. Stouffer, G. A. Meehl, An overview of CMIP5 and the experiment design. *Bull. Am. Meteorol. Soc.* **93**, 485–498 (2012).
16. J. Sillmann, V. V. Kharin, X. Zhang, F. W. Zwiers, D. Bronaugh, Climate extremes indices in the CMIP5 multimodel ensemble: Part 1. Model evaluation in the present climate. *J. Geophys. Res. Atmos.* **118**, 1716–1733 (2013).
17. J. Sillmann, V. V. Kharin, F. W. Zwiers, X. Zhang, D. Bronaugh, Climate extremes indices in the CMIP5 multimodel ensemble: Part 2. Future climate projections. *J. Geophys. Res. Atmos.* **118**, 2473–2493 (2013).
18. Intergovernmental Panel on Climate Change, “2014: Summary for policymakers” in *Climate Change 2014: Impacts, Adaptation, and Vulnerability. Contribution of Working Group II to the Fifth Assessment Report of the Intergovernmental Panel on Climate Change*, C. B. Field, *et al.*, Eds. (Cambridge Univ Press, 2014), pp. 1–32.
19. S. Fuss, *et al.*, Betting on negative emissions. *Nat. Clim. Chang.* **4**, 850–853 (2014).
20. N. S. Diffenbaugh, *et al.*, Quantifying the influence of global warming on unprecedented extreme climate events. *Proc. Natl. Acad. Sci.* **114**, 4881–4886 (2017).
21. P. A. Stott, *et al.*, Attribution of extreme weather and climate-related events. *Wiley Interdiscip. Rev. Clim. Chang.* **7**, 23–41 (2016).
22. D. R. Easterling, K. E. Kunkel, M. F. Wehner, L. Sun, Detection and attribution of climate

extremes in the observed record. *Weather Clim. Extrem.* **11**, 17–27 (2016).

23. J. M. Wallace, C. Deser, B. V. Smoliak, A. S. Phillips, Attribution of Climate Change in the Presence of Internal Variability. *World Sci. Ser. Asia-Pacific Weather Clim.* **6**, 1–29 (2016).

24. G. Hegerl, F. Zwiers, Use of models in detection and attribution of climate change. *Wiley Interdiscip. Rev. Clim. Chang.* **2**, 570–591 (2011).

25. B. B. Sarojini, P. A. Stott, E. Black, Detection and attribution of human influence on regional precipitation. *Nat. Clim. Chang.* **6**, 669–675 (2016).